Coupling of impurity modes in one-dimensional periodic systems

P. Royo, R. P. Stanley, and M. Ilegems
Institut de Micro- et Optoélectronique, Ecole Polytechnique Fédérale de Lausanne, CH 1015, Lausanne EPFL, Switzerland
(Received 24 November 2000; published 19 June 2001)

One-dimensional periodic dielectric structures are known to exhibit band gaps because of their symmetry. Defect states can be found in the band gaps if an impurity layer is added to the lattice such that the symmetry of the structure is broken. In this paper, we consider the case where a second impurity layer is added and we discuss the existence of coupling between the two defects. We discuss the possibility of exploiting the coupling of impurity modes in the realization of tunable wavelength emitting devices and dual-wavelength vertical-cavity surface-emitting lasers.

DOI: 10.1103/PhysRevE.64.016604 PACS number(s): 42.70.Qs, 42.50.−p, 42.55.Sa, 42.60.Da

I. INTRODUCTION

Several papers have already highlighted the analogy between the traditional distributed Bragg reflector (DBR) and the one-dimensional photonic crystal [1–3]: the stop band of the DBR can be considered as an energy gap or a photonic band gap (PBG), in which no mode can exist in the crystal. It was shown in Ref. [4] that a variable-width layer placed inside a one-dimensional periodic structure can create impurity photon states within the photonic band gap. Within this formalism a perfect Fabry-Pérot cavity is identical to a mid-gap impurity mode. It is well known that changing the thickness of the impurity layer shifts the energy of the defect state. Recently, coupled-cavity structures have attracted much interest for realization of dual-wavelength laser emission [5–7]. Dual-section vertical cavity surface-emitting lasers (VCSELs) have also been used to obtain wavelength tuning [8,9]. These structures can be considered as one-dimensional periodic structures having two impurity layers. The purpose of this paper is to discuss the existence of defect states in such structures and to investigate how they couple. It is easy to calculate the electromagnetic modes of such a structure using standard techniques (transfer matrices), but this tells us little about the general behavior of impurity modes and how they couple. Therefore we use a PBG type formalism to treat the general case of two defect layers of which a coupled cavity is just one manifestation.

II. UNPERTURBED ONE-DIMENSIONAL PERIODIC STRUCTURE

The structure we study is given in Fig. 1. It is based on a DBR structure with alternating $\lambda_{Bragg}/4$ layers of GaAs and AlAs, where $\lambda_{Bragg}=950$ nm is the Bragg wavelength. At this wavelength the refractive indices of GaAs and AlAs are $n_2=3.54$ and $n_1=2.96$, respectively, and the index contrast is defined as $n=n_2/n_1>1$. The corresponding thicknesses of the layers are $L_2=\lambda_{Bragg}/4n_2$ and $L_1=\lambda_{Bragg}/4n_1$. We consider two impurity layers of normalized thicknesses ξ_1 and ξ_2 defined such that their physical thicknesses are $L_{c1}=\xi_1\lambda_{Bragg}/n_1$ and $L_{c2}=\xi_2\lambda_{Bragg}/n_2$. These layers are placed symmetrically $P-0.5$ layers away from the edges of the structure and separated by $C=N-2P+0.5$ periods (see Fig. 1). The integers P and C correspond to the number of low index n_1 layers.

Let us first consider the case of the unperturbed structure with $\xi_1=\xi_2=1/4$ and $N-0.5=2P+C-0.5$ periods. The photonic band structure can be completely determined by solving a master equation [3]: in one-dimensional structures and for on-axis propagation, some energy gaps can be found for which no modes can exist in the crystal. Our purpose is to discuss the existence of defect states inside these gaps. For that purpose, the use of transmission (or reflection) coefficients provides enough information. The traditional approach to calculating these parameters is to use transfer matrix theory [10].

By using this formalism, the complex reflection and transmission coefficients of the unperturbed structure can be expressed as $r_N=|r_N|e^{i\varphi_N}$ and $t_N=|t_N|e^{i(\varphi_N+\pi/2)}$. These coefficients depend on the number of periods N, the index contrast n, and the normalized energy $\tilde{E}=\lambda_{Bragg}/\lambda$ (we consider on-axis propagation, hence the angular and polarization dependences are not to be considered here). For lossless structures, the energy conservation is expressed by the relation $|r_N|^2+|t_N|^2=1$. The complex reflection and transmission coefficients can be shown to be invariant under a normalized energy translation of $2q$: $r_N(\tilde{E})=r_N(\tilde{E}+2q)$ and $t_N(\tilde{E})=t_N(\tilde{E}+2q)$ with q integer.

By using Bloch-Floquet's theorem [10], it is possible to show that a plane wave cannot propagate in the unperturbed structure if its normalized energy is in the band gaps defined by the intervals $[\tilde{E}_N^-+2q,\tilde{E}_N^++2q]$ centered on the integers $1+2q$ with $\tilde{E}_N^-=(1/\pi)\arccos\{[(n-1)^2-4n\cos(\pi/N)]/(n+1)^2\}$ and $\tilde{E}_N^+=2-\tilde{E}_N^-$. The integers $q=0,1,2,\ldots$ correspond to band numbers with increasing energies. The energy width of the band gaps is completely determined by the index contrast n and the number of periods N, and hence does not depend on the band number q. In what follows, we consider the case of the first band only; hence $q=0$.

It is well known [10] that close to the Bragg condition $\tilde{E}=1+2q$ the amplitude of the complex reflection and transmission coefficients of a DBR can be assumed to be constant in energy, provided the number of periods and the index contrast are sufficiently high. The phase can also be considered to vary linearly with respect to the normalized energy.

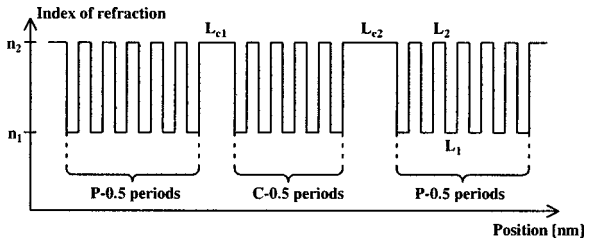

FIG. 1. Schematic of the one-dimensional periodic structure investigated in this paper. The indices of refraction are displayed as functions of the position. The high and low indices of refraction correspond, respectively, to GaAs and AlAs (evaluated at 950 nm). The two impurity layers have variable thicknesses L_{c1} and L_{c2}.

We can then approximate r_N and t_N by

$$r_N = \varrho_N e^{i D_N(\tilde{E}-1-2q)}, \tag{1}$$

$$t_N = \tau_N e^{i D_N(\tilde{E}-1-2q)+i\pi/2} \tag{2}$$

for normalized energies in the stop band $[\tilde{E}_N^-, \tilde{E}_N^+]$. The constant $\varrho_N=(n^{2N}-1)/(n^{2N}+1)$ is the amplitude of the complex reflection coefficient at the Bragg condition, and D_N is given by [11]

$$D_N = \frac{\pi}{2}\left[\left(\frac{n+1}{n-1}\right)\varrho_N - 1\right]. \tag{3}$$

This parameter can be related to an equivalent penetration depth of the electromagnetic field inside the mirror [12]. It increases continuously with the number of period N and saturates to the value $\pi/(n-1)$ when N tends to infinity.

III. ONE-DIMENSIONAL PERIODIC STRUCTURE WITH TWO DECOUPLED IMPURITY LAYERS

Let us then consider the structure given in Fig. 1 with two impurity layers of arbitrary thicknesses $\xi_{1,2}$. Using the transfer matrix formalism, the transmission coefficient of the structure is

$$T = \frac{|t_C|^2|t_P|^4}{\left|[1-|r_C||r_P|e^{i\psi_1}][1-|r_C||r_P|e^{i\psi_2}]+|t_C|^2|r_P|^2e^{i(\psi_1+\psi_2)}\right|^2}, \tag{4}$$

where $r_{P,C}$ and $t_{P,C}$ are the complex reflection and transmission coefficients of unperturbed one-dimensional periodic structures with P and C periods, respectively. Using approximations (1) and (2), the phases can be expressed as

$$\psi_{1,2} = 4\pi\,\xi_{1,2}\tilde{E} + (D_P+D_C)(\tilde{E}-1), \tag{5}$$

where $D_{P,C}$ are calculated with expression (3) by replacing N with P and C, respectively.

In order to analytically find the energies of the defect states, it is necessary to determine the resonances of T. A general analytical solution of that problem is not known. However, if the two impurities are decoupled (which is the case when $C \gg P$), one can find an analytical expression of the energies $\tilde{E}_{defect}^{1,2}$ corresponding to the resonances of T:

$$\tilde{E}_{defect}^{1,2}(p_{1,2},\xi_{1,2}) = \frac{2\pi p_{1,2}+D_P+D_C}{4\pi\,\xi_{1,2}+D_P+D_C}. \tag{6}$$

These expressions correspond to the energies $\tilde{E}_{1,2}$ of a one-periodic structure with a single impurity layer of thickness $\xi_{1,2}$. Since the impurities are decoupled, two distinct sets of solutions can be found: the indexes 1 and 2 refer to the sets of solutions associated with impurities of normalized thicknesses ξ_1 and ξ_2, respectively. The integers $p_{1,2}$ are twice the cavity thicknesses $\xi_{1,2}$ at which the defect states are midgap impurities ($\tilde{E}_{defect}^{1,2}=1$ if and only if $p_{1,2}=2\,\xi_{1,2}$).

The relation (6) gives the normalized energies of the resonances but does not specify whether these resonances are defect states or not, that is to say, if these energies are in the band gap or not. We consider that a resonance can be associated with a defect state when its energy satisfies the condition $\tilde{E}_N^- < \tilde{E}_{1,2}(p_{1,2},\xi_{1,2}) < \tilde{E}_N^+$ (the other states are continuum resonances). This inequality can be rewritten according to $\xi_{1,2}^-(p_{1,2}) < \xi_{1,2} < \xi_{1,2}^+(p_{1,2})$ with

$$\xi_{1,2}^{\pm}(p_{1,2}) = \frac{2\pi p_{1,2}+(D_P+D_C)(1-\tilde{E}_N^{\mp})}{4\pi\tilde{E}_N^{\mp}}. \tag{7}$$

The intervals $[\xi_{1,2}^-(p_{1,2}),\xi_{1,2}^+(p_{1,2})]$ (centered on $\xi_{1,2}=p_{1,2}/2$) thus correspond to the cavity thicknesses $\xi_{1,2}$ for which defect states of energies $\tilde{E}_{defect}^{1,2}(p_{1,2},\xi_{1,2})$ can exist. We call these the allowed intervals. Their widths increase linearly with respect to the parameters $p_{1,2}$. A finite number of intervals $[\xi_{1,2}^+(p_{1,2}),\xi_{1,2}^-(p_{1,2}+1)]$ [centered on $\xi_{1,2}=(2p_{1,2}+1)/4$] can exist for which no defect states are found. We call these the forbidden intervals. Their widths decrease as $p_{1,2}$ increase; hence, for $\xi_{1,2}^+(p_{1,2}) > \xi_{1,2}^-(p_{1,2}+1)$, the allowed intervals start to overlap. The number of forbidden intervals p_0 is found to be

$$p_0 = \mathrm{ceil}\left(\frac{\tilde{E}_N^-}{\tilde{E}_N^+-\tilde{E}_N^-} - \frac{D_P+D_C}{2\pi}\right), \tag{8}$$

where the function ceil(x) rounds the real number x to the nearest integer toward plus infinity.

Figure 2 summarizes these results, using the parameters $P=15$ and $C=\infty$. With the chosen parameters, Eq. (8) gives a value of $p_0=4$; hence the allowed intervals overlap when

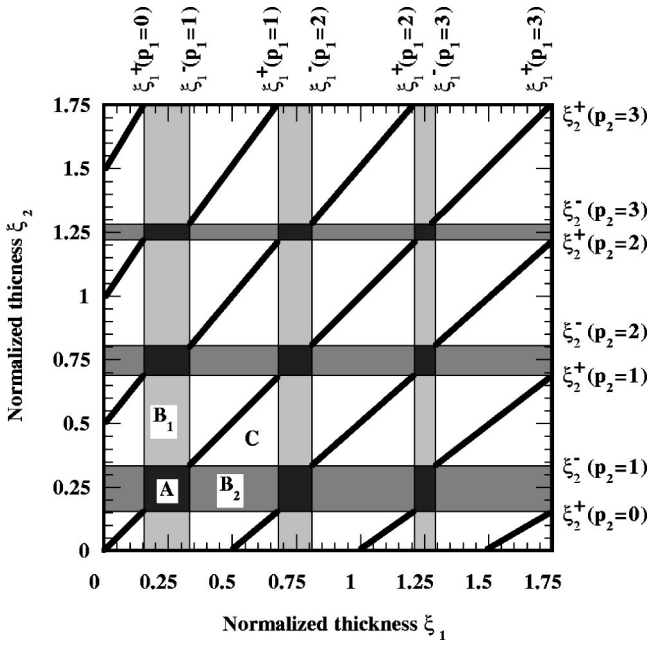

FIG. 2. First allowed and forbidden intervals of thicknesses of the two impurity layers (decoupled case). Depending on the values of $\xi_{1,2}$, four types of region can exist: A (dark gray), $B_{1,2}$ (mid and light gray), and C (white). In these regions, zero, one, or two impurity modes can respectively exist in the band gap. The dark lines correspond to the degenerate modes of the C-type regions.

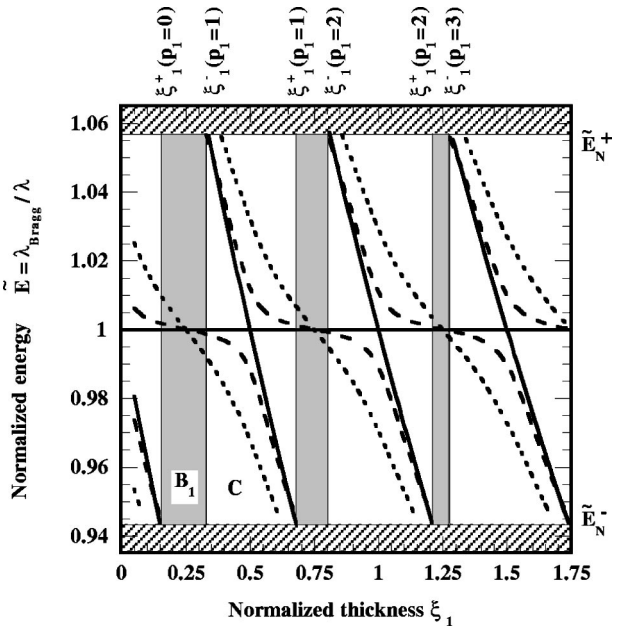

FIG. 3. Normalized energies $\tilde{E}_{a,b}$ of the defect states found for the parameters $C=3$ (dotted line), $C=8$ (dashed line), $C=\infty$ (solid line), $P=15$, $\xi_2=1$, and plotted versus ξ_1. As ξ_1 varies between 0 and 1.75, regions of type B_1 and C are scanned (gray and white areas, respectively).

$p_{1,2}>p_0+1$. Several defect states can thus exist in the band gap as soon as the impurity thickness $\xi_{1,2}$ becomes greater than the critical thickness $\xi^+_{1,2}(p_0)$. Each square of Fig. 2 corresponds to one of four possible regions of the (ξ_1,ξ_2) plane, which we call A, $B_{1,2}$, and C. The type A regions (displayed in dark gray on Fig. 2) correspond to the (ξ_1,ξ_2) values such that $\xi^+_1(p_1)\leqslant\xi_1\leqslant\xi^-_1(p_1+1)$ and $\xi^+_2(p_2)\leqslant\xi_2\leqslant\xi^-_2(p_2+1)$. For such structures, no mode exists in the band gap. The type $B_{1,2}$ regions (displayed in mid and light gray on Fig. 2) correspond to the (ξ_1,ξ_2) values such that $\xi^+_{1,2}(p_{1,2})\leqslant\xi_{1,2}\leqslant\xi^-_{1,2}(p_{1,2}+1)$ and $\xi^-_{2,1}(p_{2,1})\leqslant\xi_{2,1}\leqslant\xi^+_{2,1}(p_{2,1})$. For such structures, only one mode exists in the band gap. The type C regions (displayed in white on Fig. 2) correspond to the (ξ_1,ξ_2) values such that $\xi^-_1(p_1)\leqslant\xi_1\leqslant\xi^+_1(p_1)$ and $\xi^-_2(p_2)\leqslant\xi_2\leqslant\xi^+_2(p_2)$. For such structures, two modes can exist in the band gap. It is important to note that in this last case the two defect states are degenerate when $\tilde{E}^1_{defect}(p_1,\xi_1)=\tilde{E}^2_{defect}(p_2,\xi_2)$. Solving this equation, one finds that (ξ_1,ξ_2) belongs to the diagonals of the domains defined by the intervals $[\xi^-_1(p_1),\xi^+_1(p_1)]$ and $[\xi^-_2(p_2),\xi^+_2(p_2)]$. They are displayed as solid lines on Fig. 2. These degeneracies will be lifted by introducing some coupling between the impurities.

IV. ONE-DIMENSIONAL PERIODIC STRUCTURE WITH TWO COUPLED IMPURITY LAYERS

For that purpose we consider the case of a finite number of periods C separating the two impurity layers. We will assume ξ_2 constant and equal to 1. The second impurity layer thickness will be allowed to vary between 0 and 1.75 in order to scan several forbidden and allowed intervals of thickness and to remain in the case where only one or two defects can exist in the band gap (types B_1 and C regions).

Figure 3 displays the normalized energies of the defect states found for structures with $C=3$ (dotted line), $C=8$ (dashed line), and $C=\infty$ (solid line) periods separating the impurity layers. The band gap of these structures corresponds to the interval of normalized energies $[\tilde{E}^-_N,\tilde{E}^+_N]$ (the hatched area of Fig. 3 indicates the limits of the band gap). The decoupled case ($C=\infty$) is treated using Eq. (6): the defect state of the second impurity has an energy $\tilde{E}^2_{defect}(p_2,\xi_2)$ constant and equal to 1. The energy of the first defect state $\tilde{E}^1_{defect}(p_1,\xi_1)$ decreases as the thickness ξ_1 increases. The gray and white areas in Fig. 3 correspond to the regions of type B_1 and C, for which one and two defect states can be found, respectively. The boundaries of these intervals can be calculated by using Eq. (6) in the decoupled case ($C=\infty$).

The two defect states are degenerate at the positions $\xi_1=p_1/2$ with p_1 integer. When the two impurities are coupled, this degeneracy is lifted producing an anticrossing. These curves are calculated by using exact simulations based on the transfer matrix method. The splitting energy can be analytically calculated for perfectly symmetrical structures only $(\xi_1=\xi_2=1)$, giving [10]

$$\Delta\tilde{E}=\frac{2}{D_C+D_P+4\,\pi}\arccos\left(\frac{|r_C|(1+|r_P|^2)}{2|r_P|}\right). \qquad (9)$$

As pointed out in [5], the splitting occurs only when $|r_C|<2|r_P|/(1+|r_P|^2)$, which shows that, if the reflectivity

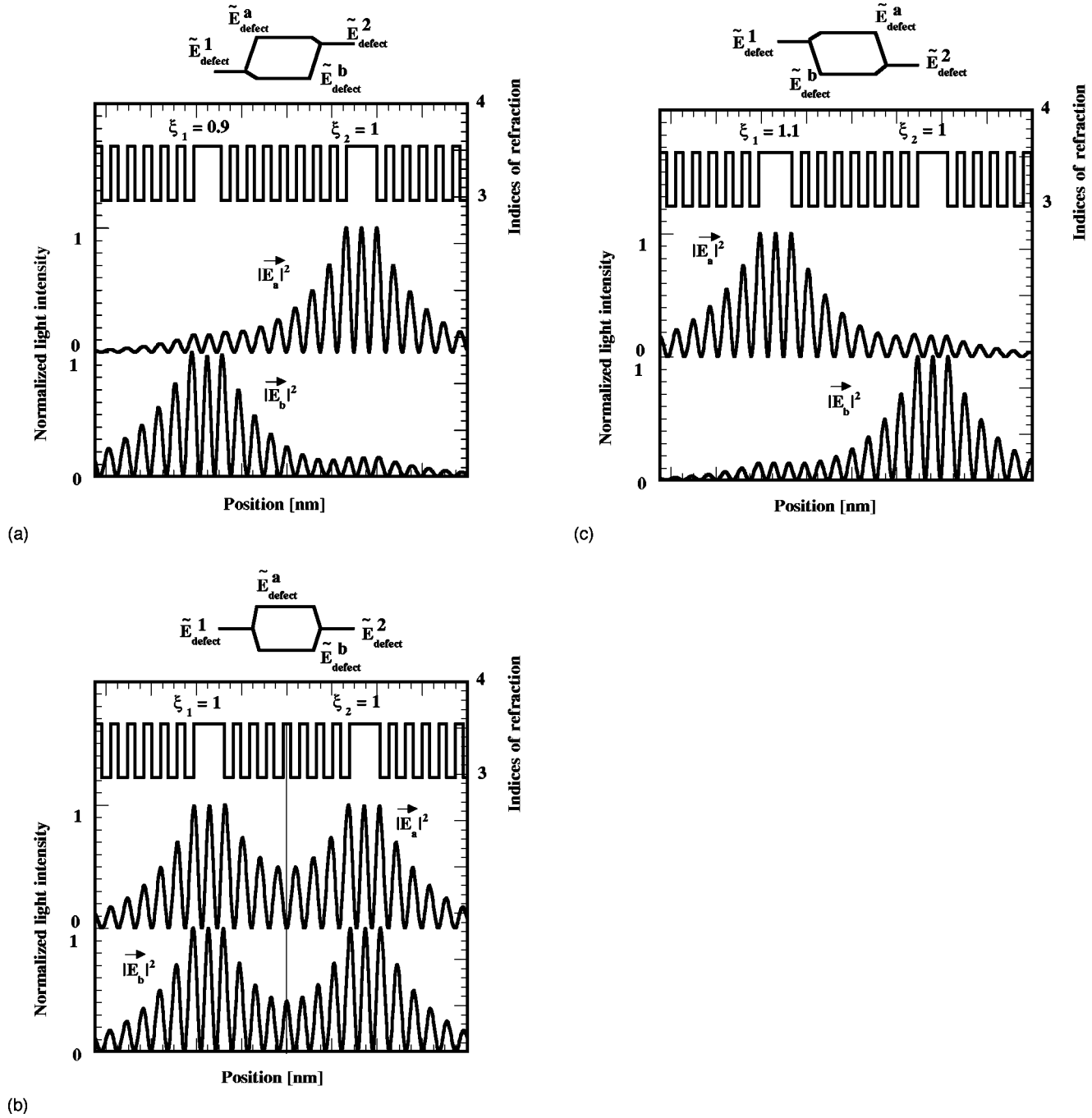

FIG. 4. Intensities $|\vec{E}_a|^2$ and $|\vec{E}_b|^2$ of the electromagnetic fields calculated at the normalized energies $\tilde{E}^a_{defect}$ and $\tilde{E}^b_{defect}$, respectively, and plotted with respect to the position (left-hand axes). The refractive indices of the structures are displayed on top of the figures (right-hand axes). The parameters of the structures are $C=8$, $P=15$, $\xi_1=0.9$ (a), $\xi_1=1$ (b), $\xi_1=1.1$ (c), and $\xi_2=1$. A schematic of the defect energies in the coupled and decoupled cases is represented on top of each figure.

of the coupling structure $|r_C|$ is smaller than the outer structure reflectivity $|r_P|$, then a splitting will always be visible (provided that $\xi_1=\xi_2=1$). Equation (9) shows that the splitting energy increases with increasing coupling strength between the two impurities, which shows up in Fig. 3 (the coupling decreases as the number of periods C increases). This behavior is in exact analogy to that of two coupled quantum states for which the energy splitting is proportional to the coupling between the electron wave functions of each state. Note that the boundaries of the forbidden intervals of thickness $[\xi_1^+(p_1),\xi_1^-(p_1+1)]$ enlarge as the coupling increases because the degeneracy splitting tends to repel the two branches away from $\xi_1=p_1/2$.

For the decoupled structure, the defect states of energies $\tilde{E}^1_{defect}(p_1,\xi_1)$ and $\tilde{E}^2_{defect}(p_2,\xi_2)$ are precisely localized in the impurity layers of thicknesses ξ_1 and ξ_2, respectively.

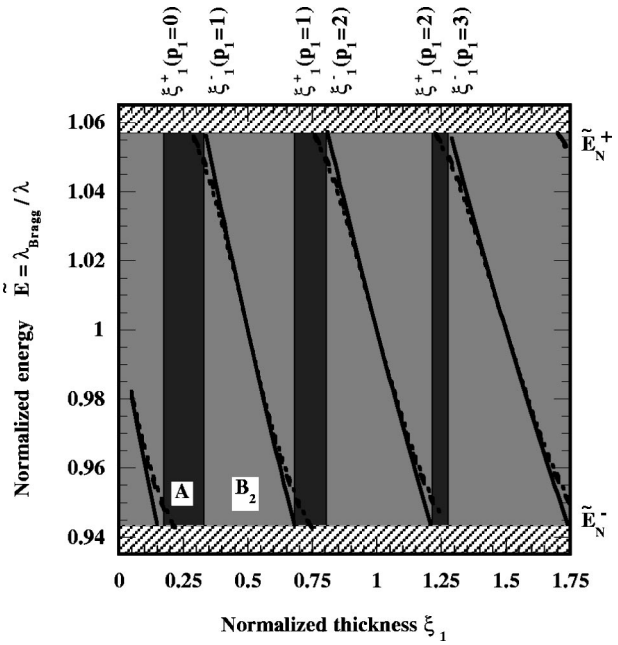

FIG. 5. Normalized energies $\tilde{E}_{a,b}$ of the defect states found for the parameters $C=3$ (dotted line), $C=8$ (dashed line), $C=\infty$ (solid line), $P=15$, $\xi_2=0.75$ and plotted versus ξ_1. As ξ_1 varies between 0 and 1.75, regions of type A and B_2 are scanned (dark and light gray areas, respectively).

When the two defects are coupled, the degeneracy of states with energies $\tilde{E}^{1,2}_{defect}(\xi_1=p_1/2,p_2=1)$ is lifted and two states with different energies $\tilde{E}^{a}_{defect}$ and $\tilde{E}^{b}_{defect}$ are created. These states are then no longer completely localized in a single impurity layer. Defining $\tilde{E}^{a}_{defect}$ and $\tilde{E}^{b}_{defect}$ as the high and low energy states, respectively, we can consider them as antibonding and bonding states in analogy to the coupling between two discrete energy levels in the quantum theory.

Figures 4(a), 4(b), and 4(c) display on their left hand axis the (normalized) amplitudes of the electric fields $|\vec{E}_{a,b}|^2$ calculated for the normalized energies $\tilde{E}_{a,b}$ for $(\xi_1=0.9,\xi_2=1)$, $(\xi_1=1,\xi_2=1)$, and $(\xi_1=1.1,\xi_2=1)$, respectively. The refractive indices of the structures are displayed on the right hand axes of these figures. On top of each graph are shown the energies $\tilde{E}^{1,2}_{defect}$ and $\tilde{E}^{a,b}_{defect}$ of the decoupled and coupled states, respectively. Figure 4(a) shows that the antibonding and bonding states are mainly confined in the impurity layers of thicknesses ξ_1 and ξ_2, respectively, which is not surprising. Considering Fig. 3 at $\xi_1=0.9$, the antibonding and bonding states clearly originate from the decoupled states related to the impurity layers of thicknesses ξ_1 and ξ_2, respectively. The contrary is observed in Fig. 4(c) for the same reason: the antibonding and bonding states are mainly localized in the impurities of thicknesses ξ_2 and ξ_1, respectively. Note that the localization of the electric fields $|\vec{E}_{a,b}|^2$ in the impurity layers decreases as the coupling gets stronger. Figure 4(b) shows that when $\xi_1=\xi_2=1$ the defect states are equally spread in both impurity layers. The thin vertical line indicates that these two states have opposite symmetry: as can be expected from the analogy to two coupled quantum states, the bonding state is symmetric and the antibonding state is antisymmetric.

Figure 5 displays the normalized energies of the defect states found for structures with $C=3$ (dotted line), $C=8$ (dashed line), and $C=\infty$ (solid line) periods separating impurity layers of thicknesses ξ_1 (variable) and $\xi_2=3/4$ (fixed). As in Fig. 3, the band-gap limits are indicated by horizontal lines at $\tilde{E}=\tilde{E}_N^{\pm}$. As ξ_1 increases from 0 to 1.75, regions of types A and B_2 (represented in Fig. 5 as dark and light gray areas, respectively) are scanned. Because one mode can exist at most, the energy of the impurity mode does not depend on the coupling strength. The defect state (when it exists) is always localized in the impurity layer of thickness ξ_1, whatever ξ_1 is.

V. PRACTICAL APPLICATIONS

Considering Fig. 2, four kinds of structure can be realized with different mode properties (provided the impurity layer thicknesses are such that $p_{1,2}<p_0+1$ as previously mentioned). Structures of type A display a mirrorlike behavior and correspond to distributed Bragg reflectors. Structures of type $B_{1,2}$ exhibit a single mode in the band gap and are used for realization of vertical cavity surface-emitting lasers when operated in the stimulated regime [13] and resonant cavity light-emitting diodes [14] when operated in the spontaneous regime.

Considering the results displayed in Figs. 3 and 5, one sees that it is possible to shift the energies of the defect states by changing the thickness of one impurity layer while keeping the thickness of the other constant. This effect has important practical applications in realization of densely packed two-dimensional arrays of multiwavelength-emitting VCSELs used in wavelength division multiplexing systems. In type B_2 structures, one impurity layer has a fixed thickness $\xi_2=(1+2\,p_2)/4$ (p_2 integer) whereas the second impurity layer is tuned around $\xi_1=p_1/2$ (p_1 integer) so as to shift the energy of the single defect state in the band gap. Typically $\xi_2=1/4$ and ξ_1 is tuned around 1 [4]. This solution is difficult to use in practice because the tuning layer has to be also the active layer (the electromagnetic field of the defect state is indeed almost completely localized in this layer). Hence changing its thickness is difficult to perform without introducing some nonradiative recombination centers. This type of structure is generally fabricated by using unconventional growth techniques with variation of the growth conditions (temperature, for example) over the wafer [8] or *in situ* masking techniques [15].

In type B_1 structures, one impurity layer has a fixed thickness $\xi_2=p_2/2$ (p_2 integer) whereas the second impurity layer is tuned around $\xi_1=(1+2p_1)/4$ (p_1 integer) so as to shift the energy of the single defect state in the band gap. Typically $\xi_2=1$ and ξ_1 is tuned around 1/4 or 3/4. These structures are of great interest because they offer the possibility of

strongly localizing a single impurity mode in one layer and controlling its energy by adjusting the thickness of the other impurity layer. This makes possible practical control of the tuning layer thickness without degrading the active impurity layer. Because of the coupling between the two defect states represented in Fig. 3, the degeneracy of the two impurity modes at $\xi_1 = p_1/2$ is lifted, which modifies the slope of the $\tilde{E}^{a,b}_{defect}(\xi_1)$ curves at $\xi_1 = (1+2\,p_1)/4$ with p_1 integer. This slope is zero for the decoupled case ($C=\infty$), and increases up to a maximum when the coupling is the strongest ($C=1$). The tunability is maximum when $p_1 = 0$ and decreases as p_1 increases, which is not surprising because of Eq. (6). Many practical applications of such structures can be found in the literature. The modification of the thickness of the tuning layer can be obtained by oxidation techniques [9,16] or etch and regrowth techniques [17,18], for example.

For structures of type *C*, the two modes existing in the band gap are partially localized in each impurity layer, which makes possible realization of dual-wavelength laser emission as demonstrated by [6] and [19]. By choosing active-passive configurations, it is also possible to design numerous devices like integrated optical disk readout heads using a VCSEL with an intracavity quantum-well absorber [20], coupled resonator vertical cavity lasers for modulation of the output power [21], or three-contact VCSELs demonstrating applications like optical intensity modulation, phase and amplitude modulation of a microwave optical subcarrier, optical bistability, or self-pulsation [22].

VI. CONCLUSION

In conclusion, in this paper we have studied the existence of coupled impurity modes in a one-dimensional periodic structure. We have shown that for decoupled impurities simple analytical expressions can be obtained allowing one to predict the number of defect states in the band gap and their energies. The case of coupled impurities is numerically investigated and can be simply predicted assuming that the degeneracy of decoupled states is lifted by the coupling. A simple analogy between two coupled impurities and two coupled quantum levels shows that for symmetrical structures the highest energy state can be identified as an antisymmetric antibonding state, whereas the lowest energy state can be identified as a symmetric bonding state. The impurity mode coupling approach explains also when and why wavelength tunability can be expected for vertical cavity surface-emitting structures.

ACKNOWLEDGMENTS

One of the authors (P.R.) would like to acknowledge Michael Moser (Avalon Photonics Ltd, Badenerstrasse 569, CH-8048 Zurich, Switzerland) for launching this line of study and for helpful discussions. This work was supported under a joint Centre Suisse d'ELectronique et de Microtechnique (CSEM) (Switzerland) and Ecole Polytechnique Fédérale de Lausanne (EPFL) (Switzerland) program, and by the European Commission within the framework of the ESPRIT-SMILED Program.

[1] E. Yablonovitch, Phys. Rev. Lett. **58**, 2059 (1987).
[2] E. Yablonovitch and T. J. Gmitter, Phys. Rev. Lett. **63**, 1950 (1989).
[3] J. D. Joannopoulos, R. D. Meade, and J. N. Winn, *Photonic Crystals* (Princeton University Press, Princeton, NJ, 1995), p. 38.
[4] R. P. Stanley, R. Houdré, U. Oesterle, M. Ilegems, and C. Weisbuch, Phys. Rev. A **48**, 2246 (1993).
[5] R. P. Stanley, R. Houdré, U. Oesterle, M. Ilegems, and C. Weisbuch, Appl. Phys. Lett. **65**, 2093 (1994).
[6] J. F. Carlin, R. P. Stanley, P. Pellandini, U. Oesterle, and M. Ilegems, Appl. Phys. Lett. **75**, 908 (1999).
[7] M. Brunner, K. Gulden, R. Hövel, M. Moser, J. F. Carlin, R. P. Stanley, and M. Ilegems, IEEE Photonics Technol. Lett. **PTL-12**, 1316 (2000).
[8] W. Yuen, G. S. Li, and C. J. Chang-Hasnain, IEEE Photonics Technol. Lett. **PTL-8**, 4 (1996).
[9] A. Fiore, Y. A. Akulova, J. Ko, E. R. Hegblom, and L. A. Coldren, Appl. Phys. Lett. **73**, 282 (1998).
[10] P. Yeh, *Optical Waves in Layered Media* (Wiley, London, 1988).
[11] P. Royo, Ph.D. thesis 2216, Ecole Polytechnique Fédérale de Lausanne, 2000.
[12] D. I. Babic and S. W. Corzine, IEEE J. Quantum Electron. **QE-28**, 514 (1992).
[13] K. Iga, S. Ishikawa, S. Ohkouchi, and T. Nishimura, Appl. Phys. Lett. **45**, 348 (1984).
[14] E. F. Schubert, Y. H. Wang, A. Y. Cho, L. W. Tu, and G. J. Zydzik, Appl. Phys. Lett. **60**, 921 (1992).
[15] H. Saito, I. Ogura, and Y. Sugimoto, IEEE Photonics Technol. Lett. **PTL-8**, 1118 (1996).
[16] D. L. Huffaker and D. G. Deppe, IEEE Photonics Technol. Lett. **PTL-8**, 858 (1996).
[17] T. Wipiejewski, M. G. Peters, E. R. Hegblom, L. A. Coldren, IEEE Photonics Technol. Lett. **PTL-7**, 727 (1995).
[18] S. Y. Hu, E. R. Hegblom, and L. A. Coldren, Electron. Lett. **34**, 189 (1998).
[19] P. Pellandini, R. P. Stanley, R. Houdré, U. Oesterle, and M. Ilegems, Appl. Phys. Lett. **71**, 864 (1997).
[20] J. A. Hudgings, S. F. Lim, G. S. Li, W. Yuen, K. Y. Lau, and C. J. Chang-Hasnain, IEEE Photonics Technol. Lett. **PTL-11**, 245 (1999).
[21] A. J. Fischer, K. D. Choquette, W. W. Chow, H. Q. Hou, and K. M. Geib, Appl. Phys. Lett. **75**, 3020 (1999).
[22] J. A. Hudgings, R. J. Stone, C. H. Chang, S. F. Lim, K. Y. Lau, and C. J. Chang-Hasnain, IEEE J. Sel. Top. Quantum Electron. **JSTQE-5**, 512 (1999).